International Journal of Heat and Mass Transfer 192 (2022) 122921

Contents lists available at ScienceDirect

International Journal of Heat and Mass Transfer

journal homepage: www.elsevier.com/locate/hmt

Investigating the wet-to-dry expansion of organic fluids for power generation

Martin T. White

Thermo-Fluids Research Centre, School of Mathematics, Computer Science and Engineering, City, University of London, Northampton Square, London, EC1V 0HB, United Kingdom

ARTICLE INFO

Article history:
Received 1 December 2021
Revised 24 February 2022
Accepted 9 April 2022

Keywords:
Two-phase expansion
Wet-to-dry expansion
Organic Rankine cycle
Radial turbine
Waste-heat recovery

ABSTRACT

The successful and economic conversion of waste heat into electricity requires new, innovative, power cycles to be developed. The proposed wet-to-dry cycle, in which the working fluid transitions across the saturation dome during expansion, has been shown to offer significant thermodynamic benefits. However, the feasibility of achieving wet-to-dry expansion when non-equilibrium effects, which are expected during a high-speed two-phase expansion, are taken into account has not been previously established. This paper first introduces a simple method to assess the thermodynamic potential of a fluid for the wet-to-dry cycle, which confirms that the siloxanes MM and MDM are excellent contenders and under ideal conditions can achieve second law efficiencies approaching 90% whilst operating with heat-source temperatures around 200 °C. The second part of this paper presents a one-dimensional nozzle design tool that accounts for thermal and mechanical non-equilibrium effects, which has been verified against previous studies and non-equilibrium computational-fluid dynamic simulations of the two-phase expansion of the refrigerant R1233zd(E). The model is then applied to the wet-to-dry expansion of MM under operating conditions directly relevant for the wet-to-dry cycle. The results firstly indicate the importance of accounting for non-equilibrium effects when designing nozzles for wet-to-dry expansion and the importance of having a realistic model that accounts for the break-up of droplets during the expansion. More importantly, the results reveal that for eight of the twelve cases considered it is still possible to achieve the full vapourisation of the working fluid within the nozzle when non-equilibrium effects are considered. This confirms the potential of the wet-to-dry cycle to enhance the performance of waste-heat recovery systems, which, in turn, necessitates further investigation, including experimental investigation, to further explore the concept.

1. Introduction

The continued reliance of industrial processes on non-renewable fuel sources to operate, and the subsequent rejection of heat to the environment, represents a significant environmental concern. Although it is extremely difficult to quantify the exact amount of waste heat available, it has been estimated that 54 PWh of heat below 300 °C is available per year globally [1], whilst 300 TWh is available per year in the EU at temperature levels below 200 °C (33%), between 200 and 500 °C (25%) and above 500 °C (42%) [2]. As such, it is widely acknowledged that waste-heat recovery technologies are required to capture and convert that heat into other useful forms, as evidenced by the growing funding initiatives, such as those at the European [3] and national levels [4]. Whilst these technologies encompass technologies for direct heat recovery, alongside technologies such as heat pumps or chillers, the ability to generate electricity remains one of the most significant opportunities and commercial power systems based on the organic Rankine cycle (ORC) are available on the market [5], typically for heat-source temperatures below a few hundred degrees Celsius, whilst supercritical CO_2 systems being widely seen as a promising candidate for higher temperatures [6]. However, despite advances, these systems are not yet widely implemented, mainly due to high costs. As such, there remains a need for innovative systems with enhanced performance.

From a theoretical perspective, particularly for relatively low temperature waste-heat sources that can be cooled down to close to ambient conditions, the ideal thermodynamic cycle is the trilateral flash cycle [7,8], which initiates expansion from a saturated liquid state. However, the realisation of this cycle poses some difficulties, particularly around the need for expansion machines that

E-mail address: martin.white@city.ac.uk

https://doi.org/10.1016/j.ijheatmasstransfer.2022.122921

Nomenclature

Symbols

α	volume fraction
β	wet-to-dry feasibility parameter
ΔT_p	heat exchanger pinch point, K
$\dot{m}$	mass-flow rate, kg/s
$\dot{W}$	power, J/s
η_{II}	second law efficiency
$\mathfrak{h}$	heat-transfer coefficient, W/(m^2 K)
Nu	Nusselt number
Oh	Ohnesorge number
Pr	Prandtl number
Re	Reynolds number
We	Weber number
μ	dynamic viscosity, Pa s
ρ	density, kg/m^3
σ	surface tension, N/m; molecular complexity
σ_M, σ_I, σ_E, σ_Q	interfacial exchange terms
A	area, m^2
a	speed of sound, m/s
b	passage height, m
C_D	drag coefficient
c_p	specific-heat capacity at constant pressure, J/(kg K)
D	droplet diameter, m
F	interfacial force, m
h	specific enthalpy, J/kg
k	thermal conductivity, W/(m K)
L	axial length, m
N_D	droplet numer, m^{-3}
o	throat width, m
p	pressure, Pa
q	vapour quality
R	specific gas constant, J/(kg K); degree of reaction
s	specific entropy, J/(kg K)
T	temperature, K
U	overall heat-transfer coefficient, W/(m^2 K)
u	velocity, m/s
V_r	volumetric isentropic expansion ratio
x	nozzle position, m

Subscripts

$*$	throat conditions
0	stagnation conditions
cr	critical point
ex	exchanged phase
h	heat source
L	liquid
max	maximum
p	pump
sat	saturated conditions
spn	spinodal
th	throat
ts	total-to-static
V	vapour

Abbreviation

ORC	organic Rankine cycle

can tolerate two-phase conditions, which typically rules out turbomachinery. Notably then, most work in the past decades has considered volumetric expansion machines [9–11]; albeit with their limitations of relatively low efficiencies and low built-in volumetric expansion ratios which may limit their application range.

Whilst the traditional consensus is to neglect turbomachinery for two-phase expansion, based on the premise that any droplets present within the rotor will cause erosion, it has been hypothesised that modifications to the cycle could make the use of turbomachinery possible. One such option, named here as the *wet-to-dry cycle*, relies on molecularly complex working fluids that allow a two-phase expansion process to transition across the saturation dome and end in the superheated vapour region. This idea was originally explored by Elliott [12,13] who investigated the wet-to-dry expansion of toluene, although despite promising results, the concept does seem to have been taken further. More recently this idea has gained a little more traction, which could partly be driven by the need to identify more innovative waste-heat recovery technologies, but also the fact that molecularly complex working fluids, such as siloxanes [14–16] and Novec 649 [17,18], are being more widely considered for ORC systems. These recent investigations include those by the current author focussing on cycle optimisation and preliminary turbine design for the wet-to-dry cycle [19] and also investigating the performance of existing single-phase ORC turbines under two-phase inlet conditions [20], and others such as Sampedro and Védie [21] who investigated wet-to-dry cycles as a topping cycle for high-temperature waste-heat recovery. The cycle optimisation studies confirm the thermodynamic potential of the cycle, whilst the turbine design and numerical simulations, which were conducted under the assumption that the liquid and vapour phases remain at thermal and mechanical equilibrium (i.e., homogeneous thermal equilibrium), give some indication that a wet-to-dry expansion can be achieved within the stator.

However, during the high-speed two-phase expansion process that is expected within a turbine intended for wet-to-dry expansion it is not clear to what extent non-equilibrium effects play. For example, when moving to a non-equilibrium simulation the drag forces that act on the liquid droplets will result in slip, whilst the thermal resistance on both sides of the liquid-vapour interphase will ultimately reduce the rate of mass and energy exchange between the liquid and vapour. This will move the wet-to-dry transition further downstream than predicted by the homogeneous thermal equilibrium model, but the extent to which this occurs is unknown. Previously, non-equilibrium models have been widely applied to the simulation of problems such as steam flashing flows [22,23], and condensation in steam turbine stages [24]. More recently, there has also been a growing number of studies concerning two-phase effects in supercritical CO_2 compressors [25,26] and also ejectors within refrigeration systems [27,28]. However, to date, and to the author's knowledge, there have not been any detailed investigations into the feasibility of the wet-to-dry expansion cycle considering realistic two-phase expansions where non-equilibrium effects are accounted for. Moreover, there have yet to be any clear guidelines on selecting fluids for the wet-to-dry cycle. With this in mind, this paper aims to achieve three things, namely: (i) to propose some simple methods to assess the feasibility of the wet-to-dry cycle and identify suitable working fluids; (ii) to develop a quasi-1D model that can be used to design wet-to-dry expansion nozzles accounting for non-equilibrium effects; and (iii) to use this model to assess whether wet-to-dry expansion processes can be achieved using working fluids and cycle conditions that are of direct relevance to the wet-to-dry cycle.

2. Fluid and thermodynamic cycle aspects

2.1. Wet-to-dry feasibility parameter

Fluid selection is an important aspect within the design of any ORC system, and the proposed wet-to-dry cycle is no different. In

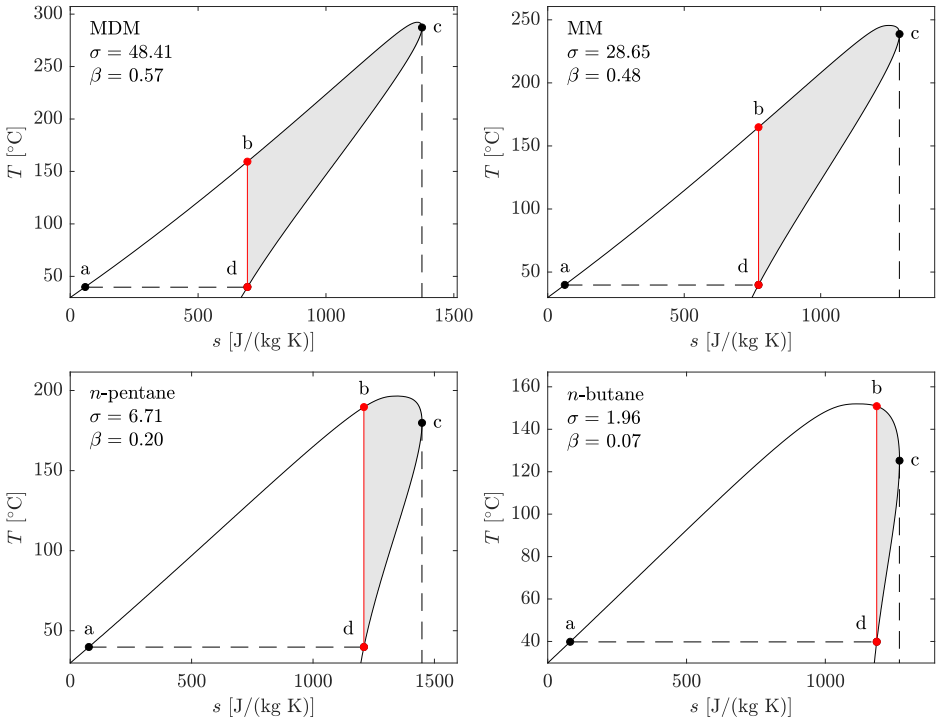

Fig. 1. Calculation of the wet-to-dry feasibility parameter β for four organic fluids. The shaded region represents conditions that allow an isentropic expansion from two-phase conditions to a saturated or superheated vapour. Results are based on a condensation temperature of 40 °C; σ refers to the molecular complexity.

fact, within this cycle fluid selection is even more restricted since only fluids with a saturated vapour line with a positive gradient when viewed in the temperature-entropy ($T - s$) plane, typically referred to as 'dry' fluids, are applicable.

To assess the suitability of a particular fluid for wet-to-dry expansion a new fluid parameter, β, is introduced, which is hereto referred to as the *wet-to-dry feasibility parameter*. This parameter is a non-dimensional parameter that determines the extent to which a particular fluid is suitable for wet-to-dry expansion. In this context, a feasible operating point is considered to be one in which expansion from a two-phase inlet condition, to a defined static pressure, results in saturated or superheated vapour at end of that expansion process. Such an expansion process could, at least at a theoretical level, be realised within a wet-to-dry ORC system. The wet-to-dry feasibility parameter essentially denotes the fraction of two-phase inlet conditions that allow an isentropic expansion to saturated or superheated vapour. If $\beta \to 0$ for a particular fluid, there is no two-phase inlet condition that can generate saturated or superheated vapour following an isentropic expansion and that fluid cannot be considered for the wet-to-dry cycle. Likewise, if $\beta \to 1$, then almost every two-phase inlet condition can result in saturated or superheated vapour following an isentropic expansion and that fluid is an excellent candidate for the wet-to-dry cycle. The wet-to-dry feasibility parameter is best understood by considering Fig. 1. For a defined ORC condensation temperature, denoted by the line a–d, it can be observed that any two-phase inlet condition to the right of the isentrope denoted b–d will permit an isentropic expansion that ends with either saturated or superheated vapour conditions, whilst an expansion from any condition to the left will remain within the saturation dome. Thus, β can be defined as the ratio of the shaded-grey area (b–c–d–b), to the area contained by the points a–b–c–d–a. Expressed mathematically, it can be defined as:

$$\beta = \frac{\int_{s_b}^{s_c} T_{sat}(s_{sat})\ \mathrm{d}s_{sat} - \int_{s_d}^{s_c} T_{sat}(s_{sat})\ \mathrm{d}s_{sat}}{\int_{s_a}^{s_c} T_{sat}(s_{sat})\ \mathrm{d}s_{sat} - \int_{s_d}^{s_c} T_{sat}(s_{sat})\ \mathrm{d}s_{sat}}, \tag{1}$$

where s_{sat} and T_{sat} denote the saturation temperature and entropy respectively. The conditions at points a, b and d can be readily obtained for a specified condensation temperature, whilst the point c corresponds to the point at which the saturated vapour entropy is at a maximum. Equation (1) is computed numerically after having first constructed a single array of s_{sat} and T_{sat} values that combines both the saturated liquid and saturated vapour entropies and passes in order through the points a, b, c and d.

The wet-to-dry feasibility parameter for four working fluids is presented in Fig. 1. These four fluids include two siloxanes and two alkanes and have been selected to demonstrate how β is related to the shape of the saturation dome. Clearly, MDM and MM are promising candidates for the wet-to-dry cycle with values of β of 0.57 and 0.48 respectively, whilst the alkanes allow wet-to-dry expansion for only a limited range of operating conditions.

It is worth noting that working fluids are often categorised by the slope of their saturation curve, as demonstrated by Chen et al. [29]. One parameter proposed for this classification is the one introduced by Invernizzi et al. [30], and later used by others [31], which is referred to as the parameter of molecular complexity, σ, which is defined as:

$$\sigma = \frac{T_{cr}}{R}\left(\frac{\partial s}{\partial T}\right)_{s_V,\ T_r=0.7}, \tag{2}$$

where T_{cr} is the critical temperature, R is the specific gas constant, s_V is the saturated vapour entropy and T_r is the reduced temperature defined as T/T_{cr}. This parameter is related to the reciprocal of the gradient of the saturated vapour line in the $T - s$ plane. Since working fluids with increasing molecular complexity have a saturation curve with an increasingly large overhang when viewed in the $T - s$ plane, an increase in molecular complexity leads to a reduction in the slope of the saturated vapour line, and thus its reciprocal (i.e., $\partial s/\partial T$) increases, leading to an increase in σ. Thus, since increasing values of σ are consistent with an increase in molecular complexity and an increase in the overhang of the saturation dome, it is apparent that σ and β are closely related and fluids

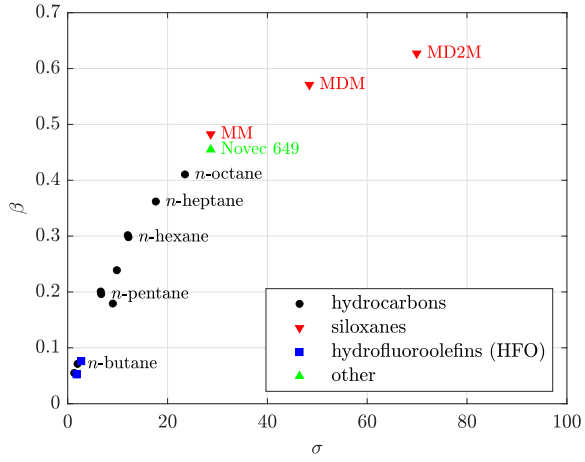

Fig. 2. Relationship between molecular complexity σ and the wet-to-dry feasibility parameter β for a range of common organic fluids. Results are based on a condensation temperature of 40 °C.

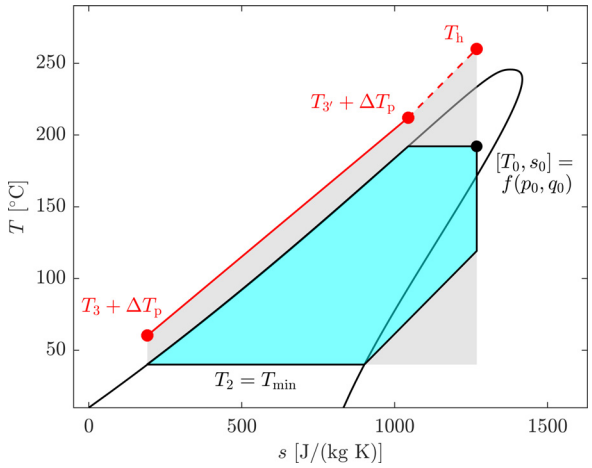

Fig. 3. A schematic of the simple wet-to-dry cycle model.

with a high molecular complexity will have a high value for β. This is confirmed by the values of σ reported in Fig. 1, whilst the relationship between σ and β is explored for a wider range of fluids in Fig. 2. Ultimately, the relationship between σ and β confirms that fluids with the highest molecular complexity are likely to be the most promising fluids for wet-to-dry expansion. Moreover, siloxanes are promising candidates for the wet-to-dry cycle, which further supports previous thermodynamic cycle optimisation results that have identified MM and MDM as two of the most promising fluids for this type of system [19].

As a final point, it is worth noting that given the relationship between σ and β it could be argued that the assessment of the suitability of a particular fluid for the wet-to-dry cycle could be completed purely based on an assessment of σ. However, the introduction of β is considered preferential for the following reasons: (i) firstly, it is a direct measure of the feasibility of two-phase expansion whilst σ was never intended for the purpose; and (ii) since β is dependent on the assumed ORC condensation temperature its use allows a slightly more detailed comparison of working fluids for a specific application.

2.2. A simple second-law assessment

Alongside selecting the right fluid, it is also important to establish the operating conditions that are the most interesting for the wet-to-dry cycle, and thus identify expansion processes of practical relevance. To this end, a simple thermodynamic model has been developed that is able to identify the optimal heat-source temperatures to which the wet-to-dry cycle could be applied and establish its theoretical potential from a second-law perspective. The required inputs are the working fluid, the minimum cycle temperature T_{min}, the turbine inlet conditions, defined in terms of a total pressure p_0 and vapour quality q_0, and an assumed heat-exchanger pinch point temperature difference ΔT_p. Since the aim of the model is to establish the theoretical potential of the cycle, compression and expansion processes are assumed to be isentropic. Thus, based on the specified inputs, the conditions at turbine inlet, turbine outlet, pump inlet and pump outlet, denoted 0, 1, 2 and 3 respectively, are readily determined.

It is well established that the best thermodynamic performance in waste-heat recovery applications is obtained when the heat-source is cooled down as much as possible and a close temperature match between the waste-heat source and working fluid is obtained in the heater, and it is in applications such as this where the largest benefits of two-phase expansion can expected. Therefore, for this simple assessment it is assumed that the temperature difference within the preheater remains approximately constant, and this is equal to ΔT_p. Thus, an energy balance applied to the preheating section yields:

$$\frac{\dot{m}}{(\dot{m}c_p)_h} = \frac{(T_{3'} + \Delta T_p) - (T_3 + \Delta T_p)}{h_{3'} - h_3} = \frac{T_{3'} - T_3}{h_{3'} - h_3}, \tag{3}$$

where $\dot{m}$ and $(\dot{m}c_p)_h$ are the working fluid mass-flow rate and heat-source heat capacity rate respectively, T and h correspond to temperature and specific enthalpy respectively, and the subscript 3' refers to the saturated liquid state at the end of the preheater.

The corresponding heat-source inlet temperature T_h follows from an additional energy balance applied to the partial evaporation process:

$$T_h = T_{3'} + \Delta T_p + \frac{\dot{m}}{(\dot{m}c_p)_h}(h_0 - h_{3'}), \tag{4}$$

whilst the power output from the cycle, expressed per unit of heat-source heat capacity rate, follows from:

$$\frac{\dot{W}}{(\dot{m}c_p)_h} = \frac{\dot{m}}{(\dot{m}c_p)_h}[(h_0 - h_1) - (h_3 - h_2)]. \tag{5}$$

Then, taking the minimum cycle temperature as the dead-state, the maximum available power, also referred to as the exergy of the heat source, is given as:

$$\frac{\dot{W}_{max}}{(\dot{m}c_p)_h} = (T_h - T_2) - T_2 \ln\left(\frac{T_h}{T_2}\right), \tag{6}$$

and the second-law efficiency of the cycle can be stated as:

$$\eta_{II} = \frac{\dot{W}}{\dot{W}_{max}}. \tag{7}$$

A schematic of this model is provided in Fig. 3, in which the wet-to-dry cycle is shown by the cyan-shaded region and the red line indicates the heat-source temperature profile. The shaded grey area indicates the irreversibility within the system.

Using this model, the performance of the wet-to-dry cycle can be investigated for different working fluids, and for different turbine inlet conditions. To demonstrate this, the model has been applied to the full range of turbine inlet conditions that allow a feasible wet-to-dry expansion using the siloxane MM, as shown by the shaded area in the top-right plot of Fig. 1. The results from the analysis are presented in Fig. 4 in which the top-left and top-right plots correspond to the optimal heat-source temperature and second-law efficiency respectively, whilst the bottom-left plot reports the volumetric expansion ratio of the isentropic expansion

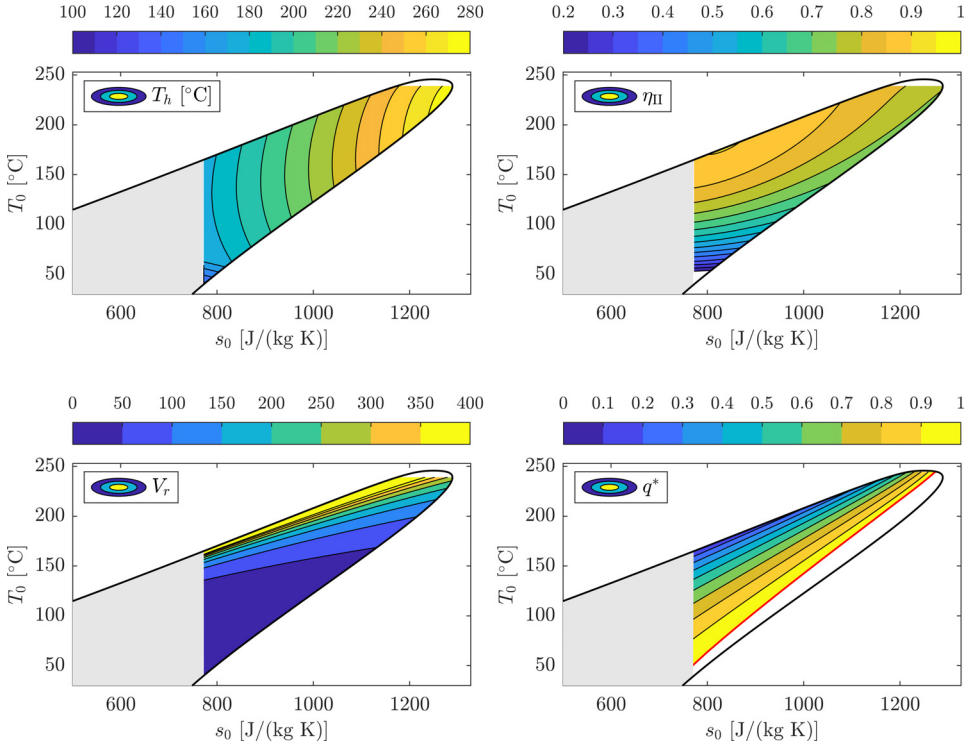

Fig. 4. Results from the cycle analysis of the wet-to-dry cycle operating with MM for different two-phase inlet conditions. Top-left: optimal heat-source temperature T_h; top-right: second-law efficiency η_{II}; bottom-left: isentropic expansion volumetric ratio V_r; and bottom-right: critical vapour quality q^* under homogeneous equilibrium assumption.

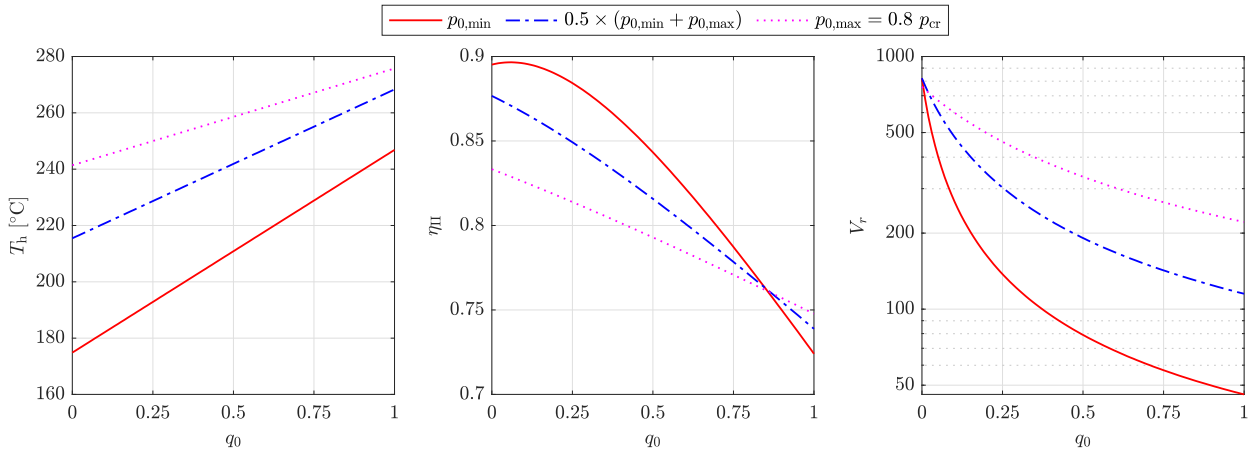

Fig. 5. Results from the cycle analysis of the wet-to-dry cycle operating with MM for different inlet vapour qualities and inlet pressures. The pressure levels correspond to 4.78, 10.12 and 15.45 bar.

(i.e., ρ_0/ρ_1). The bottom-right plot reports the critical vapour quality q^*, which is obtained under the assumption of homogeneous equilibrium between the two phases and is helpful to understand whether the conditions downstream of nozzle throat are expected to be single- or two-phase. The same results are also reported as a function of inlet vapour quality and inlet pressure in Fig. 5 to aid interpretation, where $p_{0,min}$ is the minimum pressure at which a full wet-to-dry transition can occur and corresponds to an inlet pressure of 4.78 bar.

From the results, the first observation is that for a given pressure, expanding from the lowest inlet vapour quality will lead to the highest second-law efficiency. Moreover, the best performance point corresponds to expansion from the minimum pressure, defined by $p_0(q_0, s_L = s_V|_{T_{sat}=T_{min}})$. At this point, a very close match between the working fluid and the heat source is obtained, leading to a cycle that is very close to an ideal cycle with a very high second law efficiency. Subsequently, it can be said that for operation with MM there is a single heat-source temperature at which this high second law efficiency can be obtained, and this corresponds to around $T_h \approx 180$ °C. Increasing the pressure from the minimum pressure of 4.78 bar, to 10.12 and 15.45 bar causes a reduction in second law efficiency from around 90% to around 87% and 83% respectively, but subsequently allows the cycle to match heat-source temperatures of around 220 and 240 °C respectively. The downside of these highly efficient cycles is the significant increase in the isentropic expansion volumetric ratio, which approach values in excess of 500 for expansion from saturated liquid and could have consequences on the turbine design and operation. However, it is observed that a small increase in the vapour quality can cause a significant reduction in the isentropic expansion volumetric ra-

tio. Thus, for a practical system the optimal inlet vapour quality will be trade-off between maximising the performance of the cycle, and ensuring a practical turbine design can be realised.

In summary, the model presented provides a useful way to assess the potential of the wet-to-dry cycle, whilst the results reported in Figs. 4 and 5 confirm the potential of the cycle when operating with MM. The analysis was also repeated with MDM, which has a higher critical temperature and a higher value for β due a higher degree of molecular complexity. As a result, the optimal operating conditions (i.e., $p_0 = p_{0,\min}$, $q_0 = 0$) correspond to a slightly lower heat-source temperature of $T_h \approx 170$ °C, whilst the efficiency is comparable to the maximum efficiency obtained fro MM. However, it is worth noting that the corresponding inlet pressure is around 1.12 bar, whilst the required isentropic expansion volumetric ratios are almost an order of magnitude higher for expansion from saturated liquid, which rules this operating point for practical reasons. Overall, it is found that MDM only outperforms MM at heat-source temperatures above 265 °C, with second-law efficiencies of 75% and below as the heat-source temperature increases. Thus, when considering fluid and cycle perspectives at a fundamental level, the siloxane MM appears to be a strong candidate for the wet-to-dry cycle, which confirms findings from preliminary cycle simulations [19].

3. Non-equilibrium nozzle design model

3.1. Pressure profile

The nozzle design model constructs the required planar nozzle geometry for the expansion of a fluid from a defined two-phase inlet condition, defined with a stagnation inlet pressure p_0, vapour quality q_0, and initial velocity, u_0, to a specified outlet pressure p_{out} with a defined mass-flow rate, $\dot{m}$. The nozzle is sized according to input values for the passage width to throat ratio, b/o_{th}, and the length to throat ratio, L/o_{th}. Since the throat size will vary depending on the extent to which non-equilibrium effects are present, the initial sizing (i.e., determination of b and L) is conducted based on the required throat width under the assumption of homogeneous thermal equilibrium between the phases which can be easily calculated (i.e., $A_{th} = bo_{th} = \dot{m}/(\rho^* a^*)$, where ρ^* and a^* are the critical density and speed of sound of the homogeneous mixture). Thus, when designing nozzles for a given application, and where non-equilibrium effects may influence by a varying degree, the length and passage width will be the same, although there may be slight variations in the eventual throat width.

The model is based on an inverse design approach, in which the nozzle static pressure distribution is prescribed as a model input. The nozzle inlet pressure, p_{in}, is determined from the specified inlet conditions (i.e., p_0, q_0 and u_0) and the assumption that liquid and vapour phases are at thermal and mechanical equilibrium at the nozzle inlet, whilst p_{out} is a model input. The nozzle profile is then constructed using a Bezier curve with three control points, as shown in Fig. 6. It is assumed that $(\mathrm{d}p/\mathrm{d}x)|_{x=0} = (\mathrm{d}p/\mathrm{d}x)|_{x=L} = 0$, which requires $p(x_A) = p_{in}$ and $p(x_C) = p_{out}$, whilst $p(x_B) = 0.5(p_{in} + p_{out})$. Thus, the pressure distribution can be varied by adjusting the non-dimensional x-coordinates (i.e., x/L) of points A, B, and C.

3.2. Governing equations

The nozzle design model is based on the Eulerian-Eulerian approach for two-phase flows, with the assumption that the two-phase mixture is composed of dispersed liquid droplets suspended in the continuous vapour phase. For a given set of inputs, the model solves a separate set of governing equations for both the liquid and vapour phases. For quasi one-dimensional steady-state

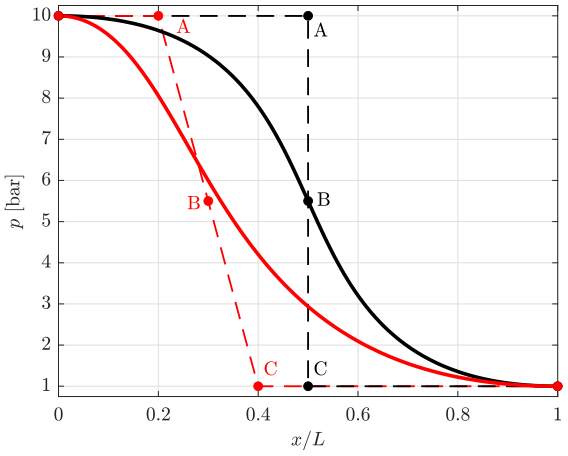

Fig. 6. Example static pressure distributions generated using a three control point Bezier curve.

flow through a duct with a varying area the governing equations for phase i can be expressed as [32]:

$$\frac{1}{A}\frac{\partial(\alpha\rho Au)_i}{\partial x} = \sigma_{M,i}; \tag{8}$$

$$[3ex]\frac{1}{A}\frac{\partial\left(\alpha\rho Au^2\right)_i}{\partial x} + \alpha_i\frac{\partial p}{\partial x} = \sigma_{J,i}; \tag{9}$$

$$[3ex]\frac{1}{A}\frac{\partial\left(\alpha\rho Au\left(h+\frac{u^2}{2}\right)\right)_i}{\partial x} = \sigma_{E,i}, \tag{10}$$

where α, ρ, h, p and u correspond to the volume fraction, density, specific enthalpy, pressure and velocity of phase i respectively, A is the channel area and σ_M, σ_J and σ_E correspond to the amount of mass, momentum and energy exchanged between the two phases.

The mass exchange term is determined by applying an energy balance to the liquid-vapour interphase [32,33]:

$$\sigma_{M,L} = -\sigma_{M,V} = \frac{\mathfrak{H}_L A_i(T_{sat} - T_L) + \mathfrak{H}_V A_i(T_{sat} - T_V)}{h_{LV}} \tag{11}$$

where $\mathfrak{H}_L$ and $\mathfrak{H}_V$ are the heat-transfer coefficients on the liquid and vapour sides of the interface, A_i is the interfacial area, T_{sat} is the saturation temperature and h_{LV} is the latent heat of vapourisation. The momentum and energy exchanges are likewise defined [32]:

$$\sigma_{J,i} = \vec{F}_i + \sigma_{M,i}u_{ex}; \tag{12}$$

$$[3ex]\sigma_{E,i} = \sigma_{Q,i} + \sigma_{M,i}\left(h_{ex} + \frac{u_{ex}^2}{2}\right), \tag{13}$$

where $\vec{F}_i$ is the interfacial force, u_{ex} and h_{ex} are the velocity and enthalpy of the exchanged phase and:

$$\sigma_{Q,L} = -\sigma_{Q,V} = UA_i(T_V - T_L), \tag{14}$$

where U is the overall heat-transfer coefficient (i.e., $1/U = 1/\mathfrak{H}_L + 1/\mathfrak{H}_V$). The interfacial force is determined from:

$$\vec{F}_L = -\vec{F}_V = A_i C_D \rho_V |u_V - u_L|(u_V - u_L), \tag{15}$$

where C_D is the drag coefficient.

3.3. Interfacial and droplet modelling

Within the nozzle design model the interfacial terms can be defined using any existing empirical correlation to determine the interfacial heat-transfer coefficients and drag coefficient. Within the current work the Ranz-Marshall correlation [34] is used to model the heat-transfer coefficient on the vapour side of the vapour-liquid interphase:

$$Nu_V = \frac{\mathfrak{H}_V D}{k_V} = 2 + 0.6 Re_D^{1/2} Pr^{1/3}, \tag{16}$$

where D is the droplet diameter, k_V is the thermal conductivity of the vapour, Pr is the Prandtl number of the vapour (i.e., $(c_p\mu/k)_V$), and Re_D is the Reynolds number:

$$Re_D = \frac{\rho_V |u_V - u_L| D}{\mu_V}, \tag{17}$$

where μ_V is the viscosity of the vapour. The model is also setup to allow a specified value for Nu_V, or the zero resistance case in which $\mathfrak{H}_V \to \infty$ and $T_V \to T_{sat}$. Likewise, on the liquid side a constant Nusselt number, or zero resistance (i.e., $T_L \to T_{sat}$), can be applied, although as an initial assumption it is assumed that [33]:

$$Nu_L = \frac{\mathfrak{H}_L D}{k_L} = 6. \tag{18}$$

The drag coefficient is determined based on the Schiller-Naumann correlation [35]:

$$C_D = \begin{cases} \frac{24}{Re_D}, & \text{if } Re_D \le 0.1 \\ \max\left[0.44, \left(\frac{24}{Re_D}\right)\left(1 + 0.15 Re_D^{0.687}\right)\right] & \text{otherwise.} \end{cases} \tag{19}$$

Referring to Eqs. (16)–(19) it is apparent that the mass, momentum and energy exchange is dependent on the size, or more specifically the diameter, of the liquid droplets. Therefore, the droplet diameter can be considered an important parameter and to obtain accurate predictions a realistic value for D is required. However, given the novelty of the current application and the lack of suitable experimental data it is difficult to select a suitable value for D. Therefore the approach adopted within this study is to consider different methods for predicting the droplet diameter, and to run a series of parametric study in which the influence of these models results can be examined.

Within the model, three different approaches have been considered, which correspond to: (i) a fixed droplet diameter; (ii) a fixed droplet number; and (iii) a critical Weber number. In approach one, the diameter of the droplets is assumed to be constant throughout the nozzle and hence the number of droplets per unit volume reduces as the volume fraction increases, and vice versa. In the second approach, the number of droplets is assumed constant and the droplets are allowed to reduce in size as the volume fraction is increased. The droplet number and droplet diameter are related through:

$$N_D = \frac{6(1 - \alpha_V)}{\pi D^3}. \tag{20}$$

On a physical level, assuming a constant droplet number may be considered more realistic as it allows the mass of a single droplet to vary according to the amount of mass and energy transferred to the surrounding vapour, whilst assuming a constant droplet number implies that a single droplet may fully vapourise, or nucleate, across an incremental pressure change. The constant droplet number has been successfully applied to the numerical simulation of steam flashing flows [22,23], although the vapour is assumed to be the dispersed phase and hence Eq. (20) refers to the bubble number, rather than the droplet number.

The third approach models the break-up of the liquid droplets according to the Weber and Ohnesorge numbers, and is commonly applied in atomisation [36]. The Weber number represents the ratio of the drag forces which disrupt a droplet to surface tension forces which resist that disruption, and is defined as:

$$We = \frac{\rho_V (u_V - u_L)^2 D}{\sigma}, \tag{21}$$

where σ is the surface tension. The Ohnesorge number represents that ratio of viscous to surface tension forces acting on a droplet and is defined as:

$$Oh = \frac{\mu_L}{\sqrt{\rho_L D \sigma}}. \tag{22}$$

At sufficiently high Weber numbers, the drag forces become sufficiently high to cause break-up of the droplets, and for $Oh < 0.1$ that break-up occurs at a constant value of $We = 11$. For $Oh < 10$, which is not exceeded within this work, the Weber number at which break-up occurs, referred to as the critical Weber number We_{cr}, is obtained from Guildenbecher et al. [36]:

$$We_{cr} = We_{cr,Oh\to 0}\left(1 + 1.077 Oh^{1.6}\right) \tag{23}$$

where $We_{cr,Oh\to 0} = 11$. Thus, for a known critical Weber number the maximum droplet number is given from:

$$D_{max} = \frac{We_{cr}\sigma}{\rho_V (u_V - u_L)^2}. \tag{24}$$

Thus, in this approach, the nozzle design model is initiated with an initial droplet size at the nozzle inlet. Then, at each location within the nozzle the maximum droplet diameter is calculated. If the maximum droplet diameter is greater than the current droplet diameter the droplet diameter remains unchanged, otherwise break-up is assumed to occur and the droplet diameter is set to the maximum droplet diameter. In this approach, N_D and D remain linked through Eq. (20), but both vary along the length of the nozzle. In practice, the results are relatively insensitive to the initial input droplet size, with changes in this parameter only affecting the calculation within the first few percent of the nozzle length.

An alternative approach would be to model the droplet break-up through the introduction of an additional differential equation to model the droplet evolution, as previously applied to flashing flows [37] and condensation in steam turbines [24] for example. However, the approaches adopted here are simple to implement within the model, and are considered a suitable first approximation.

3.4. Numerical implementation

For a specified set of thermodynamic and geometrical inputs, and for a defined pressure profile, the nozzle design model is initiated by determining the nozzle length and discretising this length into n nodes, each with a specified pressure. Then, starting at the nozzle inlet and marching forward along the length of the nozzle, the six governing equations are solved numerically at each node to determine the six flow variables, i.e., T_L, T_V, u_L, u_V, α_V and A. At each node, the first-order differential terms are obtained using the second-order accurate backward difference scheme and the numerical solution is completed using the *fsolve* function available in MATLAB's Optimisation Toolbox (v2020b). Fluid properties are modelled using the Span-Wagner Helmholtz equation of state available within REFPROP (v10), including the calculation of metastable properties; for the fluids evaluated in the following sections specific details can be found in Refs. [38] (R1233zd(E)) and [39] (MM). However, the model is also developed to work with an in-house Peng-Robinson model previously developed for ORC simulations [40] and a comparison between the models is presented later. Finally, the number if nodes is set to 250 for all simulations following a sensitivity which found model predictions with $n = 250$ were within 0.1% of those obtained for $n = 500$.

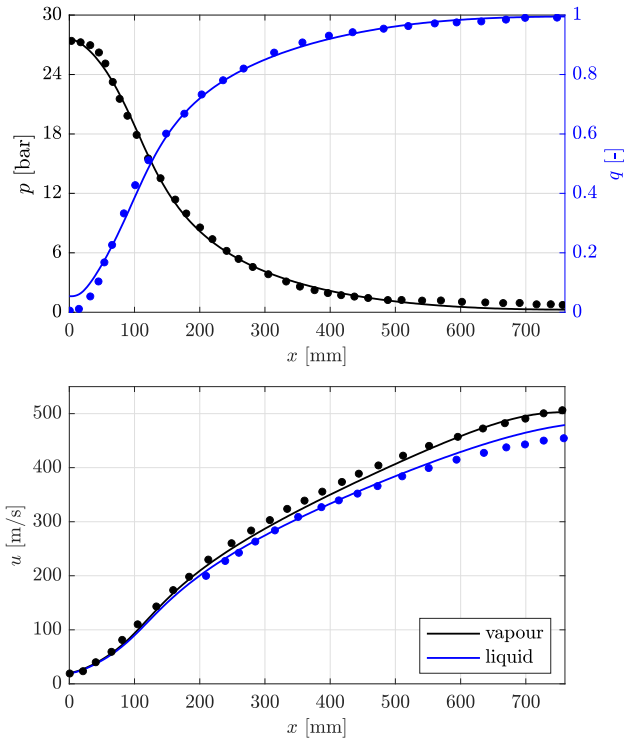

Fig. 7. Validation of the current nozzle design tool (–) against the digitised data taken from Elliott [12,13] (●). Results concern the wet-to-dry expansion of toluene from $p_0 = 28.47$ bar ($T_0 = 289$ °C) and $q_0 = 0.01$ with $\dot{m} = 1$ kg/s.

3.5. Initial model validation against Elliott

Given the relatively unique nature of the system under investigation, there are limited studies against which to validate the nozzle design tool. One exception is Elliott [12,13], who designed a wet-to-dry nozzle for the expansion of toluene. His model assumed thermal equilibrium between the two phases but accounted for slip and set the droplet diameter based on that assumption of a limiting Weber number (i.e., $We = 12$). Thus, for a fair comparison the Weber number criterion was selected to model droplet breakup, whilst Nu_L and Nu_V were set sufficiently high (i.e., $\mathcal{O}(10^3)$) to force the liquid and vapour temperatures towards the saturation temperature. A comparison between Elliott's model and those obtained using the current model is presented in Fig. 7. The pressure profile was obtained via a numerical optimisation of the Bezier control points to fit the pressure profile originally specified by Elliott.

Overall, the results reveal a good agreement between the two models, with very similar qualitative trends observed. There is a slight discrepancy in the vapour mass fraction at the inlet, which can be attributed to the assumption for the inlet velocity which is not stated in the original reference. Moreover, the current work relies on a more advanced equation of state than the ideal-gas based formulation that appears to have been used by Elliott. Nonetheless, the results reported in Fig. 7 provide good confidence in the current model.

4. Two-phase expansion of R1233zd(E)

Before progressing onto wet-to-dry expansions of fluids of interest, an investigation into the two-phase expansion of the hydrofluoroolefin, R1233zd(E), has been conducted. This fluid is considered since it is a common working fluid within low-temperature ORC systems, but also because it has a saturated vapour line that, when viewed in the $T - s$ plane, is close to vertical which means a two-phase expansion will remain within the saturation dome. This is convenient since difficulties have been encountered in reaching convergence when using non-equilibrium computational-fluid dynamic (CFD) simulations for two-phase expansion cases that transition across into the superheated region. Thus, the purpose of this investigation is twofold: (i) to provide a case study that can be evaluated via more advanced non-equilibrium CFD simulations, which can in turn provide some further validation of the nozzle design tool; and (ii) to present a case study in which the effect of varying the droplet diameter can be demonstrated.

4.1. Case study definition

The selected two-phase expansion case corresponds to the expansion of R1233zd(E) from inlet conditions of $p_0 = 20$ bar, $q_0 = 0.5$ and $u_0 = 10$ m/s to an outlet pressure of $p_{\text{out}} = 1$ bar. To be consistent with the eventual scale of the target application, which is a small-scale ORC system with a power output in the order of 100 kW, the mass-flow rate is set to $\dot{m} = 0.149$ kg/s. This is consistent with an isentropic nozzle power of 100 kW, which is subsequently divided across 16 stator vanes. The geometrical parameters for the nozzle are set to $b/o_{\text{th}} = 3$ and $L/o_{\text{th}} = 30$, whilst the non-dimensional Bezier control points are fixed at $x_A = x_B = x_C = 0.5$, which corresponds to a similar nozzle pressure distribution to that reported by the black line in Fig. 6. As noted previously, the nozzle design proceeds assuming that Nu_V is set according to the Ranz-Marshall correlation, $Nu_L = 6$ and the drag coefficient is determined based on the Schiller-Naumann correlation.

Before proceeding with the CFD validation or the parametric studies, a comparison between nozzle designs obtained using the Span-Wagner Helmholtz equation of state and the Peng-Robinson equation of state was conducted. For this comparison a number of additional two-phase expansion cases were defined, with inlet pressures ranging between 10 and 30 bar, and inlet vapour qualities ranging between 0.1 and 0.8, and the nozzle design model was run using each equation of state. More details on the expansion cases, alongside the results, are presented in the supplementary material. However, in summary it was found that under the non-equilibrium assumption, where metastable states are expected, the percentage difference in the nozzle area distributions remained below 3%, with the largest deviation observed in cases with high inlet pressures and low inlet vapour qualities. Overall, this provides some confidence in the suitability of the Helmholtz-based equation of state for modelling metastable states, and thus the subsequent results were all generated using this model.

4.2. Computational-fluid dynamic simulations

The purpose of the CFD simulations is to provide further verification of the nozzle design tool for a two-phase expansion case in which thermal and mechanical non-equilibrium are considered. For the specified thermodynamic and design inputs, and value for N_D, the nozzle design model is run and the nozzle geometry obtained on which the CFD analysis can be conducted. In keeping with the nozzle design model, the CFD simulations are based on an Eulerian-Eulerian two-phase model, and full details of the setup are provided in the supplementary material. For the two-phase expansion case corresponding to $p_0 = 20$ bar, $q_0 = 0.5$ the nozzle design was run for three different values for the droplet number, namely $N_D = 10^8$, 10^{10} and 10^{12}. The CFD simulation was then completed for each nozzle, with the droplet number set accordingly. A comparison of the results is provided in Fig. 8.

From the comparison it is observed that the pressure profile obtained from the CFD model agrees very well with the target pressure profile. Moreover, both sets of results predict similar trends in the volume fraction with axial position and with variations in N_D.

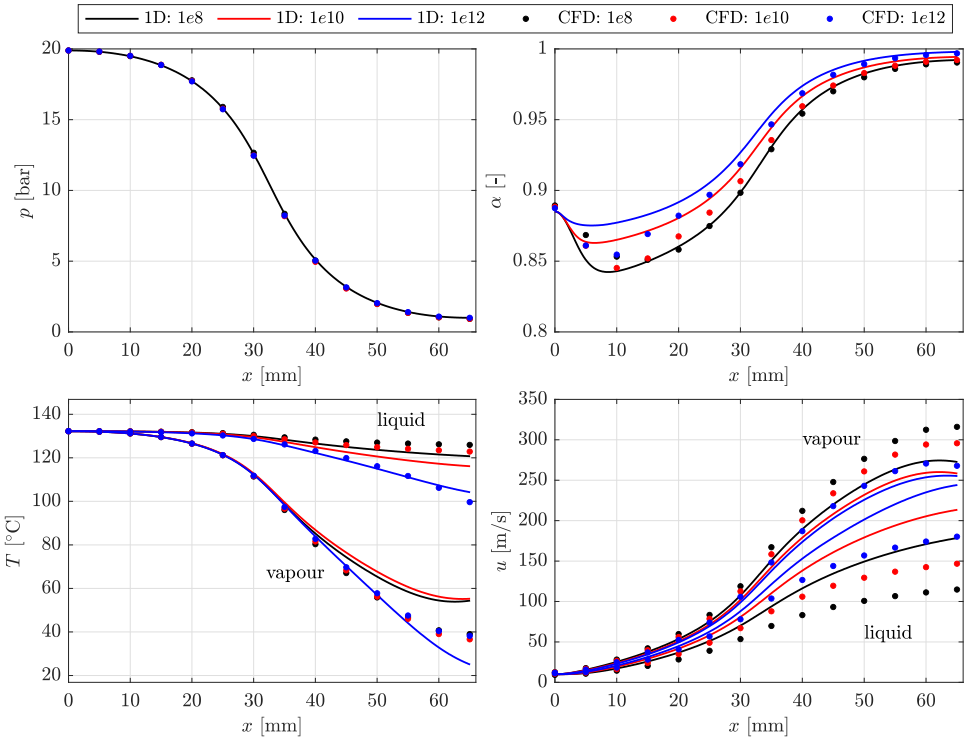

Fig. 8. Comparison between the predictions from the nozzle design model (1D) and the CFD simulations for the two-phase expansion of R1233zd(E) for $N_D = 10^8$, 10^{10} and 10^{12}.

However, overall the CFD model predicts lower volume fractions than the nozzle design model, which is consistent with the CFD model predicting a larger slip between the two phases. With respect to the evolution of the liquid and vapour temperature, a good agreement is observed, particularly with respect to the liquid temperature at increasing N_D, although the CFD simulations indicate that the vapour side is relatively insensitive to the droplet number. This could be attributed to the larger slip between the two phases, which can be expected to increase the droplet Reynolds number promoting enhanced heat transfer. As already noted, the CFD models predict a larger slip between the two phases, and ultimately, of the properties considered, the predicted liquid and vapour velocities show the largest deviations between the nozzle design and CFD models. These deviations were to be expected owing to the nozzle design model neglecting boundary layer effects, neglecting variations in the flow properties in the vertical direction, and neglecting any recirculation within the diverging part of the nozzle. Ultimately, these effects can be expected to affect the volume fraction distribution, and hence droplet diameter distribution, leading to variations in heat-transfer rates and drag forces, which may significantly influence the interfacial terms. However, it is worth noting that the same qualitative trends are observed, namely that vapour velocities reduce and liquid velocities increase as droplet number is increased. Therefore, despite the obvious limitations of the nozzle design model in accounting for the complex nature of the flow, based on the results reported here it is considered a useful tool for nozzle design and for providing a qualitative assessment of non-equilibrium effects in two-phase expansion processes relevant to power generation without resorting to complex non-equilibrium CFD simulations.

4.3. Parametric study: Effect of droplet diameter

The second part of this section aims to investigate the effect of the droplet diameter on the evolution of the flow parameters within a two-phase nozzle. For this study, the nozzle design model was run for the assumption of homogeneous thermal equilibrium (HEM), using the critical Weber number model, and for droplet numbers ranging between $N_D = 10^7$ and $N_D = 10^{15}$. The results are compared in Fig. 9, which report the evolution of pressure, area, volume and mass fraction, and temperature and velocity of the liquid and vapour phases along the non-dimensional length of the nozzle. The simulation was also repeated with the assumption of a fixed droplet diameter, rather than a fixed droplet number. The results for a fixed diameter are qualitatively similar to those reported for a fixed droplet number and for brevity are provided in the supplementary material.

The first thing to note from Fig. 9 is that at high droplet numbers (i.e., $N_D = 10^{15}$) the non-equilibrium model closely recovers the HEM solution. In other words, for high droplet numbers, where droplet diameters are also small, the rate of interfacial heat and mass-transfer exchange is high whilst the drag force is low, which drives the phases towards equilibrium. At low values of droplet number (i.e., $N_D = 10^7$), where D is increased and there is a larger resistance to heat transfer and a larger drag force, there is effectively no mass exchange between the phases and the vapour mass fraction remains unchanged along the length of the nozzle. At intermediate values of N_D, the volume fraction, liquid velocity and liquid temperature distributions transition between these two extremes. However, the evolution of the vapour temperature and vapour velocity are less clear. At low values of N_D, there is a high resistance on both sides of the liquid-vapour interface, so both mass and heat transfer are limited. Subsequently, the two phases essentially undergo separate expansions, albeit with some heat exchange which seeks to cool down the liquid and heat up the vapour. Thus, the vapour and liquid expand into the superheated vapour and metastable liquid regions respectively. As the droplet number is increased up to $N_D = 10^{11}$, and hence the droplet diameter continues to reduce, the thermal resistance on both sides of the liquid-vapour interface decreases, leading to increased mass

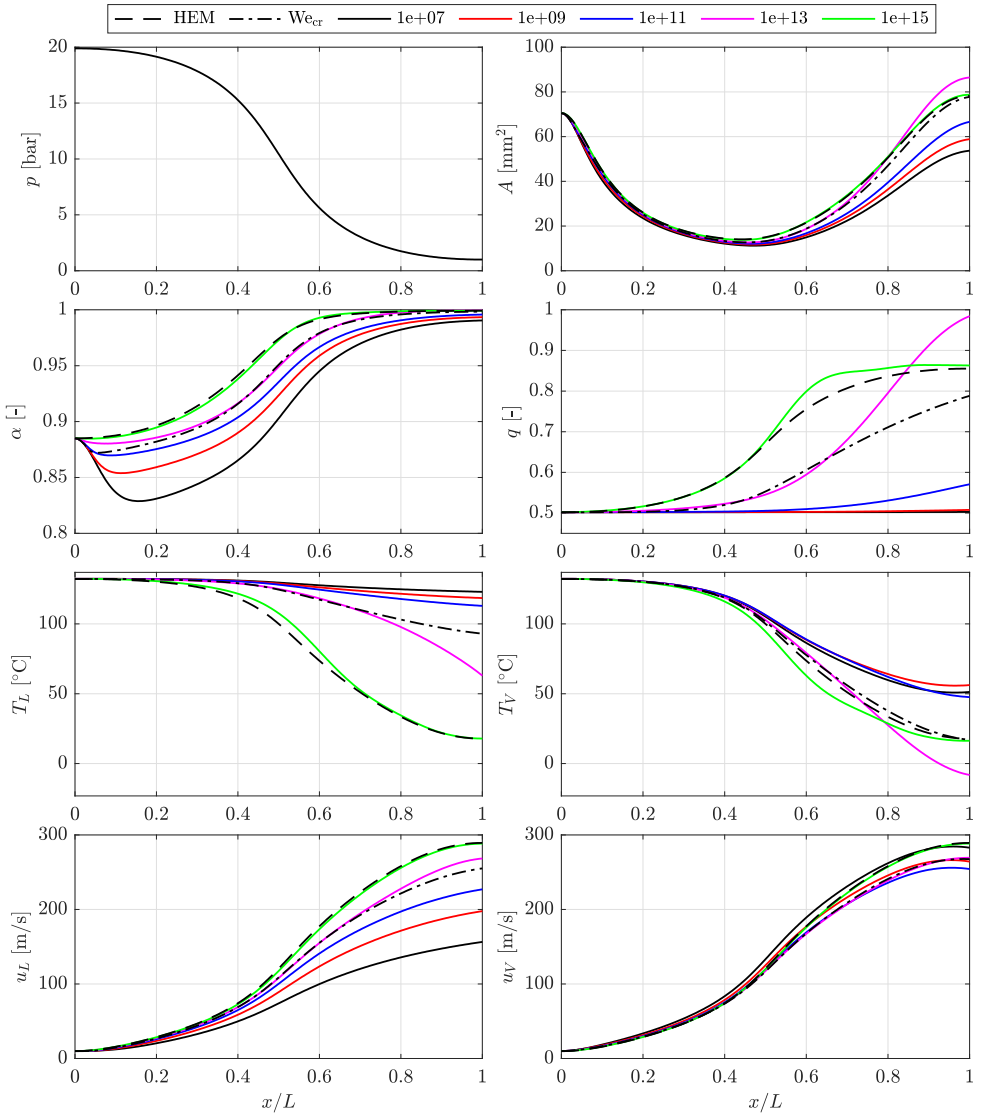

Fig. 9. Evolution of pressure p, nozzle area A, vapour volume fraction α, vapour mass fraction q, the liquid and vapour temperatures T_L and T_V, and the liquid and vapour velocities u_L and u_V along the length of the nozzle for the expansion of R1233zd(E) from $p_0 = 20$ bar and $q_0 = 0.5$ to $p_{out} = 1$ bar. The dashed line corresponds to a homogeneous equilibrium assumption, the dash-dot line corresponds to the critical Weber number model, and the coloured lines correspond to different values for N_D.

and heat transfer between the two phases. However, the resistance remains sufficiently high that the temperatures of the two phases remain away from the saturation temperature, again leading to metastable liquid and superheated vapour conditions, and a subsequent temperature difference between the two phases. As N_D is further increased, the vapour temperature appears to drop below the saturation temperature, thus becoming metastable subcooled vapour, before the homogeneous equilibrium solution is almost recovered for $N_D = 10^{15}$. Thus, it can be observed that the temperature profile of the vapour is relatively complex, and is a function of the heat-transfer coefficients on the liquid and vapour sides which are proportional to N_D, and the temperature difference between the phases which are inversely proportional to N_D. These, in turn, are path dependent and are a function of the assumed droplet number, the volume fraction and the mechanical interaction between the phases. For the high droplet number cases, it also worth noting the interesting behaviour with respect to the vapour quality and area distribution that is observed. Specifically, for the $N_D = 10^{13}$ case, higher vapour qualities, and consequently larger nozzle areas, are predicted compared to the HEM model (i.e., in the region $x/L > 0.8$). However, as N_D is further increased to 10^{15} these two parameters reduce back towards the HEM solution. At present, with the absence of studies with which to compare or validate these results, it is unknown whether this behaviour is physical, or whether this indicates a limitation of the model for these high droplet number cases. Thus, further investigation is required to establish the suitability of this approach.

Referring briefly to the results for the parametric study conducted for the fixed droplet diameter assumption, as reported in the supplementary material, the results are consistent with those obtained for the fixed droplet number assumptions. Specifically, the same trends with respect to volume fraction, liquid temperature and liquid velocity are observed, which transition from the most extreme non-equilibrium conditions for $D = 1$ mm, to the HEM conditions when the diameter is reduced to $D = 5$ μm. The trends with respect to vapour temperature, vapour velocity, vapour quality and nozzle area are also similar with the prediction of metastable vapour properties for intermediate droplet diameters.

Referring back to Fig. 9, and considering the results obtained under the critical Weber number assumption, as indicated by the dash-dot lines, it is found that this assumption does not encounter the situation encountered by the fixed droplet number model for

high values of N_D. Specifically, the critical Weber number mode leads to nozzle designs that are close to the HEM model, although there is an apparent shift in the temperature and velocity of the liquid phase compared to the HEM model. This subsequently reduces the volume and vapour mass fraction at the outlet of the nozzle. Comparatively, the vapour temperature remains close to the saturation temperature, albeit with a small degree of superheat. In other words, under the critical Weber number assumption it can be observed that whilst the predicted nozzle area is similar to that of the HEM model, and hence could have been generated under such an assumption, the presence of non-equilibrium effects can be expected to delay vapour generation, and this effect could not be predicted using the HEM model.

Ultimately, these results indicate the importance of accounting for non-equilibrium effects, and of having a realistic approximation that accounts for the break-up of the liquid droplets and allows the droplet diameter and droplet diameter to vary along the length of the nozzle. Nonetheless, in the absence of suitable experimental data it is not suitable to rely on a HEM assumption and parametric studies investigating different values of N_D can be considered a useful exercise to elaborate on the role that the droplet number, or droplet diameter, may have on the outlet conditions and the potential role of non-equilibrium effects. Moreover, in the context of wet-to-dry expansion it is clear that the performance of the nozzle can be expected to be sensitive to the inlet conditions, and specifically the droplet size and distribution at the nozzle inlet. Thus, to achieve full vapourisation it can be expected that controlling these parameters will be important.

5. Two-phase expansion of the siloxane MM

Having evaluated the two-phase expansion of R1233zd(E), the investigation is now extended to MM, which as confirmed in Section 2, is a suitable fluid for the wet-to-dry cycle. Following from the R1233zd(E) analysis, the first step is to assess the influence of the equation of state. This was done by comparing the results generated using the same two thermodynamic models as previously considered, namely the cubic Peng-Robinson and Span-Wagner Helmholtz equations of state. For both models, results were generated under the assumption of homogeneous thermal equilibrium and under the assumption of both mechanical and thermal non-equilibrium. The results were generated for different two-phase expansion processes and the results are summarised in the supplementary material. Ultimately, the results under the homogeneous equilibrium assumption are in-line with those obtained for R1233zd(E), with maximum deviations of 8% at the nozzle inlet, which quickly reduce to below 4% for $x/L > 0.05$. However, this is only for two-phase expansion from high inlet pressures. At intermediate and low pressures, the difference is below 1% for the whole nozzle. The results for the non-equilibrium case reveal very similar trends. Thus, these results indicate that the choice of thermodynamic model does not seem have a significant impact on the resulting nozzle geometry.

Having confirmed the sensitivity to the equation of state, the investigation can be extended to consider more practical wet-to-dry expansion processes. For this, 12 expansion processes have been defined, as reported in Fig. 10. These 12 cases correspond to two-phase expansion from the three inlet pressures reported in Fig. 5, namely $p_0 = 4.78$, 10.12 and 15.45 bar, and at four different inlet vapour qualities, namely $q_0 = 0.1$, 0.2, 0.3, and 0.4. The turbine outlet pressure is set based on the assumption of an ORC condensation temperature of 40 °C, and with the exception of the $p_0 = 4.78$ bar cases, the nozzle outlet (i.e., stator outlet) pressure is set assuming a degree of reaction of 0.5, calculated under the assumption of an isentropic expansion and homogeneous thermal equilibrium flow. For the $p_0 = 4.78$ bar cases, the degree of reaction was set to 0.1, 0.25, 0.4 and 0.5 for vapour qualities of 0.1, 0.2, 0.3 and 0.4 respectively. This was necessary since for these cases a higher degree of reaction would correspond to an expansion process that does not leave the saturation dome, at least under the assumption of isentropic, homogeneous thermal equilibrium flow.

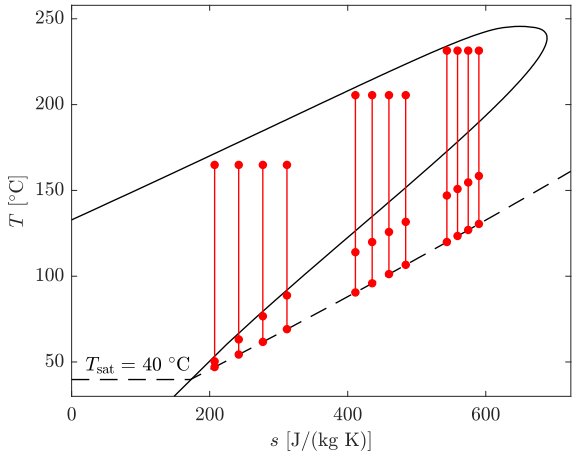

Fig. 10. Wet-to-dry expansion cases for MM. The three sets of lines correspond to inlet pressures of $p_0 = 4.78$, 10.12 and 15.45 bar respectively, at inlet vapour qualities of $q_0 = 0.1$, 0.2, 0.3, and 0.4. The intermediate point on each vertical line corresponds to the nozzle outlet condition.

For each case reported in Fig. 10, the nozzle design model was run to determine the required nozzle area distribution to achieve the desired wet-to-dry expansion. Since the primary aim of this paper is develop the nozzle design tool and investigate the feasibility of achieving a full wet-to-dry expansion when non-equilibrium effects are considered, rather than undergoing the optimisation of the nozzle geometry, the nozzle design tool is ran with the same set of design inputs as previously specified for the R1233zd(E). Specifically, the mass-flow rate is set based on an isentropic power of 100 kW, and assuming a stator with 16 stator vanes. The geometrical parameters for the nozzle are set to $b/o_{\text{th}} = 3$ and $L/o_{\text{th}} = 30$, whilst the non-dimensional Bezier control points are fixed at $x_A = x_B = x_C = 0.5$. The optimisation of these parameters is left for a later study, where suitable objective functions may be to minimise the slip velocity, the temperature between the phases, the liquid mass fraction at the nozzle outlet in the case of a completely two-phase expansion, or maximising the degree of superheat for a wet-to-dry expansion.

For the interfacial terms, it is assumed that Nu_V is set according to the Ranz-Marshall correlation and the drag coefficient is determined based on the Schiller-Naumann correlation. For the liquid side heat-transfer coefficient, it was initially assumed that $Nu_L = 6$, however as discussed in the next paragraphs this was later modified to $Nu_L = 12$. As for the assumption for the droplet diameter, various values for the droplet number or droplet diameter were attempted, but it was found that the nozzle design model was unable to reliably provide results, particularly at high values for the vapour volume fraction. However, more stable behaviour was obtained when using the third modelling approach which models droplet break-up according to the Weber number. Thus, all results presented for the MM expansion case are obtained using this droplet break-up model. Finally, it is noted that since the predominant focus of this study is confirming the location of the wet-to-dry transition point, the nozzle design model is terminated when full vapourisation is achieved (i.e., $q > 99.9$ %). The results generated for the 12 expansion cases under this set of assumptions are summarised in Fig. 11.

Before discussing the results in detail, it is worth noting that for the two $p_0 = 15.4$ bar cases with $q_0 = 0.1$ and 0.2 the model

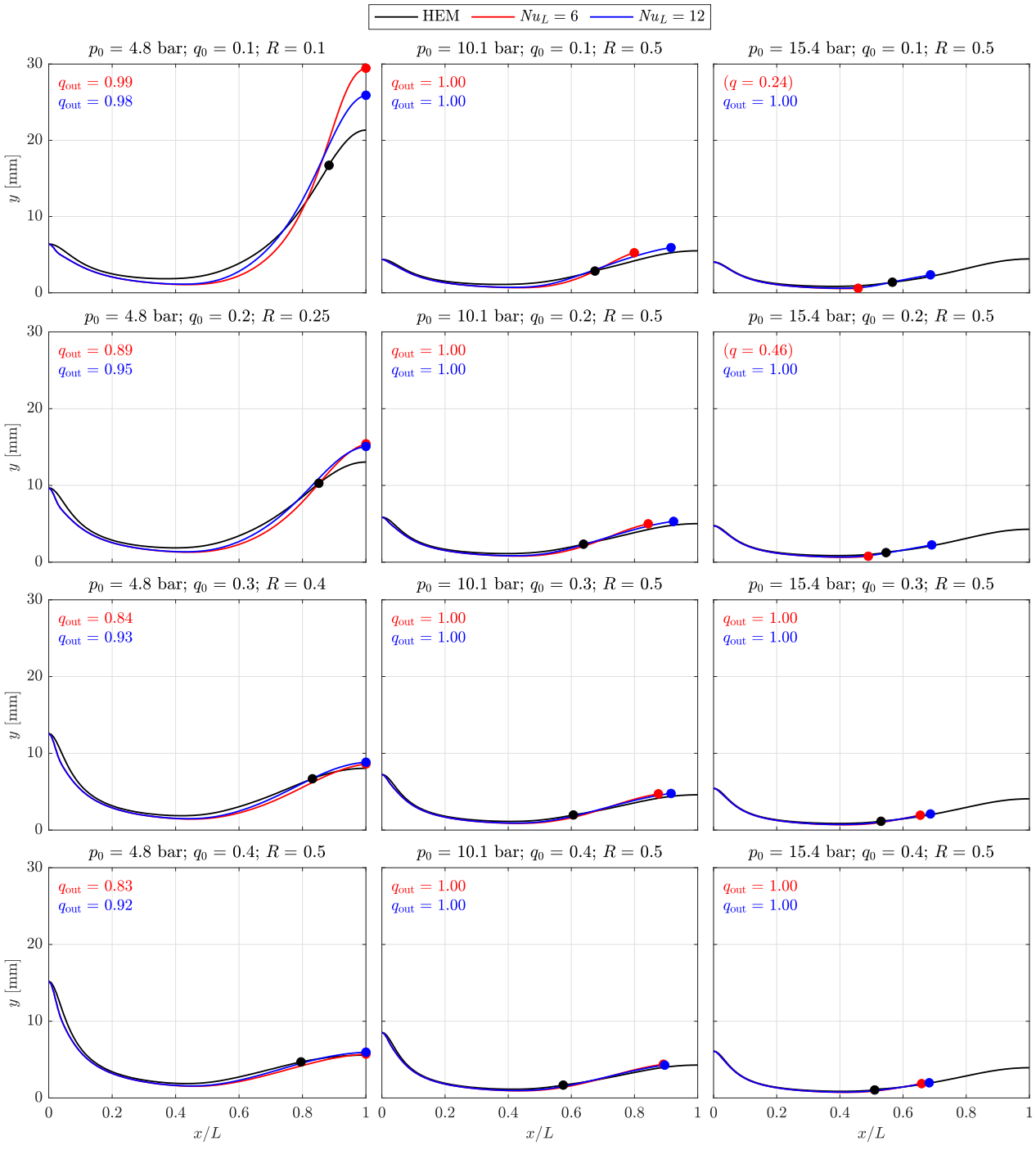

Fig. 11. Variation in nozzle half height with non-dimensional $x-$coordinate for the 12 expansion cases reported in Fig. 10. The black lines correspond to the nozzle geometry predicted under the assumption of homogeneous thermal equilibrium, whilst the red and blue lines correspond to the non-equilibrium results obtained for different values of the liquid-side Nusselt number, Nu_L. The markers (●) represents the location at which full vapourisation occurs, or the vapour quality at which the model terminates (indicated in the top left of each plot).

terminated with a vapour quality that is less than unity when $Nu_L = 6$ is assumed. Specifically, the model terminated at values of $q = 0.24$ and $q = 0.46$ respectively. The reason for this is explored in Fig. 12, which reports the difference between the fluid pressure and the corresponding spinodal pressure (i.e., calculated at the same temperature) along the length of the nozzle for different expansion cases. For expansions from low pressures (i.e., $p_0 = 4.8$ and 10.1 bar), there is a large pressure difference indicating that the metastable liquid state is far from the spinodal point. However, as the inlet pressure is increased, and the inlet vapour quality is reduced, the metastable liquid state moves closer to the spinodal limit. For the $p_0 = 15.4$ bar, $q_0 = 0.4$ and $Nu_L = 6$ case it is observed that the minimum pressure difference is obtained at $x/L = 0.5$, which, as indicated by the black pressure profile reported in Fig. 6, corresponds to the region with the highest pressure gradient and thus the region of most rapid expansion. Thus, in this region, due to the thermal resistance on the liquid side of the liquid-vapour interface that causes a delay in the heat and mass transfer, this leads to the most significant metastable states in this region. As the vapour quality is reduced further, the spinodal limit

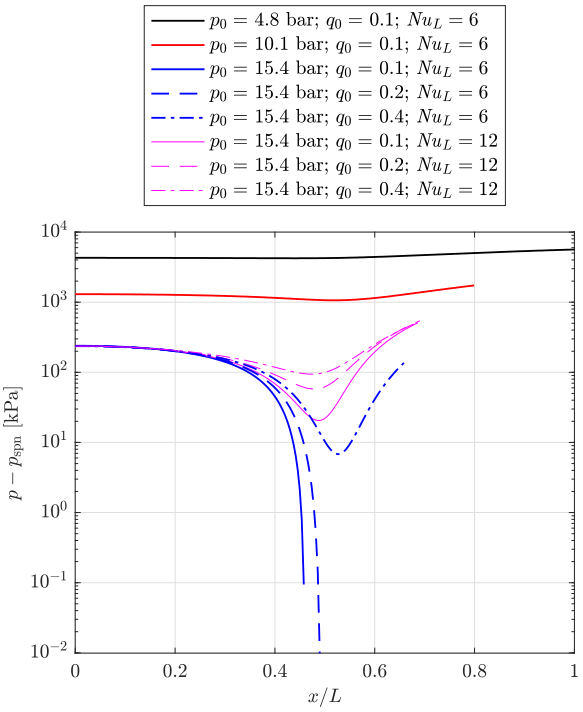

Fig. 12. Variation in the difference between the fluid pressure p and corresponding spinodal pressure of the liquid phase at the same temperature, p_{spn}, along the non-dimensional length of the nozzle for selected expansion cases.

is approached and the model fails. Thus, for these cases, the thermal resistance on the liquid side of the liquid-vapour interphase was relaxed by doubling the Nusselt number, which is equivalent to doubling the liquid-side heat-transfer coefficient. This moves the expansion process further from the spinodal and allows a solution to be obtained, as indicated in Fig. 12. Alternatively, the nozzle geometry or target pressure profile could have been modified to change the location of the maximum pressure gradient, or to reduce the gradient (i.e., by increasing the nozzle length). However, given that there remains significant uncertainty in both the suitability of the equation of state in predicting metastable states close to the spinodal limit, and in predicting a suitable value for Nu_L, the approach adopted here is considered a suitable for step.

Having discussed this, it is now suitable to analyse the results reported in Fig. 11. The first thing to note is that in all cases the consideration of non-equilibrium effects delays the vapourisation process, leading to the full vapourisation being achieved either further downstream than predicted by homogeneous equilibrium assumption, or not at all. In other words, these findings indicate that non-equilibrium effects should be considered when designing nozzles for the wet-to-dry cycle, necessitating the use of a nozzle model similar to that developed in this work.

The second observation is that for the $p_0 = 4.8$ cases it is not possible to achieve full vapourisation of the working fluid for any of the considered cases. Thus, referring to Fig. 10, where it can be seen that these two-phase expansion processes end close to the saturation dome (as also indicated in Fig. 11 by the proximity of the homogeneous equilibrium model wet-to-dry transition point to the end of the nozzle), this may indicate two things. The first is that a lower outlet pressure, and therefore smaller degree of reaction, may be necessary to achieve full vapourisation of the fluid. The second is that it can also be concluded that the most optimum cycle from a thermodynamic perspective, as indicated in Section 2, may be the hardest to achieve in practice when non-equilibrium effects are considered.

Considering the intermediate pressure cases (i.e., $p_0 = 10.1$ bar), full vapourisation of the working fluid is predicted for all cases, and this is found to occur within the last 20% of the nozzle length. Comparatively, the homogeneous equilibrium model predicts this to be achieved between 55 and 70% of the nozzle length. Similar results are also obtained for the high pressure case, namely $p_0 = 15.4$ bar. Thus, this indicates that at these pressures the wet-to-dry cycle could be feasibly deployed.

Comparing the $Nu_L = 6$ and $Nu_L = 12$ cases, it is observed that the results, or at least the location of the wet-to-dry transition, is influenced by the thermal resistance on the liquid side of the liquid-vapour interphase, and this sensitivity increases as the inlet vapour quality is reduced. This is not surprising as a low vapour quality is consistent with a lower vapour volume fraction and an increased interfacial area. Interestingly, however, the results also indicate that a higher heat-transfer coefficient on the liquid side appears to cause the wet-to-dry transition point to shift further downstream, which is perhaps counter intuitive. Upon further inspection of the results, although not presented here, it was that found a higher value for Nu_L, and hence higher heat-transfer coefficient, does lead to a a faster rate of vapour generation within the majority of the nozzle compared to the lower heat-transfer coefficient. However, in the later stages of the nozzle, the vapour generation rate for the higher heat-transfer coefficient reduces compared to the low case. This can be partly understood by noting that the mass and energy exchange between the phases is governed by the temperature differences between the liquid, vapour and saturation temperature, as well as the heat-transfer coefficients. Thus, a lower heat-transfer coefficient, which results in a larger temperature difference between the phases, particularly towards the latter stages of expansion, promotes more rapid mass and energy exchange. It is also worth noting that although the liquid-side heat transfer coefficient is generally higher than the vapour-side heat-transfer coefficient, they are both the same order of magnitude and hence neither is the controlling heat-transfer coefficient. Thus, although the liquid-side heat-transfer coefficient increases, the vapour experiences a similar resistance between the vapour and interphase in both cases.

Ultimately, the results in Fig. 11 indicate the importance of accounting for non-equilibrium effects when considering a wet-to-dry cycle operating with the fluid MM and also indicate that for 8 of the 12 cases evaluated it may be possible to successfully achieve full vapourisation of the working fluid within the nozzle. However, the results have also indicated that at the most promising operating point from a thermodynamic cycle perspective, it may not be feasible to achieve such an expansion. Thus, at the heart of the problem is a trade-off between the thermodynamic performance of the cycle and the potential to realise the required wet-to-dry expansion process in a practical nozzle.

6. Conclusions

Previous studies have indicated that the wet-to-dry cycle, in which the working fluid transitions across the saturation dome during expansion, could offer significant thermodynamic benefits compared to existing systems based on the organic Rankine cycle. Ultimately, this cycle could increase power output by up to a third, thus helping to increase the uptake of waste-heat recovery technologies and help reduce the amount of waste heat that is currently rejected to the environment. However, the feasibility of achieving a wet-to-dry expansion process has yet to be confirmed. Thus, this paper has explored the wet-to-dry expansion of organic fluids with the aim of establishing the role that non-equilibrium effects have in the expansion process, and confirming whether a wet-to-dry expansion can be achieved when these effects are considered.

The results obtained for the two-phase expansion of the refrigerant R1233zd(E) indicate the importance of accounting for non-equilibrium effects when assessing two-phase expansion, and reveal the importance of having a realistic model that accounts for the break-up of the liquid droplets. The results obtained for the wet-to-dry expansion of the siloxane MM confirm this finding, and reveal a sensitivity to the liquid side heat-transfer coefficient. In other words, it is not suitable to rely on the assumption of homogeneous equilibrium when designing nozzles for two-phase expansion, thus confirming the need for a suitable design tool that can model non-equilibrium effects. Moreover, the results reveal the importance of having accurate models to predict interfacial heat-transfer coefficients and drag forces. Thus, given the current absence of suitable experimental data, more numerical investigations and experimental testing is necessary to provide more confidence in the developed models. In the absence of such data, parametric studies can be used to assess the influence of the interfacial models.

Ultimately, the results for the wet-to-dry expansion of MM under relevant operating conditions indicate that for eight of the twelve cases considered it is possible to achieve full vapourisation of the fluid within the nozzle when non-equilibrium effects are considered. This confirms the feasibility of designing nozzles that can fulfil the requirements of the wet-to-dry cycle. However, the four cases in which wet-to-dry expansion is not possible correlate to the most preferential cycle conditions. Therefore, there is a trade-off between achieving the optimal thermodynamic performance of the cycle, and having a wet-to-dry expansion that can be achieved within a practical nozzle. Thus, an optimal cycle can only be identified after having evaluated the thermodynamic performance of the cycle and modelling the wet-to-dry expansion process accounting for non-equilibrium effects. Finally, it is commented that in the context of wet-to-dry expansion it is apparent that the performance of the nozzle will be sensitive to the nozzle inlet conditions (i.e., size and distribution of droplets), and controlling these parameters may be important in achieving the desired vapourisation.

Declaration of Competing Interest

I wish to confirm that there are no known conflicts of interest associated with this publication and there has been no significant financial support for this work that could have influenced its outcome.

Acknowledgments

This project was supported by the Royal Academy of Engineering under the Research Fellowship scheme (2019–2024). Award number: RF\201819\18\23.

Supplementary material

Supplementary material associated with this article can be found, in the online version, at doi:10.1016/j.ijheatmasstransfer.2022.122921.

References

[1] C. Forman, I.K. Muritala, R. Pardemann, B. Meyer, Estimating the global waste heat potential, Renew. Sustain. Energy Rev. 57 (2016) 1568–1579, doi:10.1016/j.rser.2015.12.192.
[2] M. Papapetrou, G. Kosmadakis, A. Cipollina, U. La Commare, G. Micale, Industrial waste heat: estimation of the technically available resource in the EU per industrial sector, temperature level and country, Appl. Therm. Eng. 138 (2018) 207–216, doi:10.1016/j.applthermaleng.2018.04.043.
[3] G. Tasiopoulos, S. Feketova, CORDIS Results Pack on Waste Heat Valorisation, Technical Report, European Commission, Luxembourg, 2020. https://cordis.europa.eu/article/id/422033-waste-heat-valorisation
[4] https://www.gov.uk/guidance/industrial-heat-recovery-support-programme-how-to-apply [Last accessed: 17/11/2021].
[5] C. Wieland, F. Dawo, C. Schifflechner, M. Astolfi, Market report on organic Rankine cycle power systems: recent developments and outlook, in: 6th International Seminar on ORC Power Systems, 11–13 October, Munich, Germany, 2021, pp. 1–10, doi:10.14459/2021mp1636584.
[6] M.T. White, G. Bianchi, L. Chai, S.A. Tassou, A.I. Sayma, Review of supercritical CO_2 technologies and systems for power generation, Appl. Therm. Eng. 185 (2021), doi:10.1016/j.applthermaleng.2020.116447.
[7] I.K. Smith, Development of the trilateral flash cycle system: Part 1: fundamental considerations, Proc. Inst. Mech.Eng. Part A 207 (3) (1993) 179–194, doi:10.1243/pime_proc_1993_207_032_02.
[8] J. Fischer, Comparison of trilateral cycles and organic Rankine cycles, Energy 36 (10) (2011) 6208–6219, doi:10.1016/j.energy.2011.07.041.
[9] I.K. Smith, N. Stosic, C.A. Aldis, Development of the trilateral flash cycle system: Part 3: the design of high-efficiency two-phase screw expanders, Proc. Inst. Mech.Eng. Part A 210 (1) (1996) 75–93, doi:10.1243/pime_proc_1996_210_010_02.
[10] H. Öhman, P. Lundqvist, Experimental investigation of a Lysholm turbine operating with superheated, saturated and 2-phase inlet conditions, Appl. Therm. Eng. 50 (1) (2013) 1211–1218, doi:10.1016/j.applthermaleng.2012.08.035.
[11] G. Bianchi, R. McGinty, D. Oliver, D. Brightman, O. Zaher, S.A. Tassou, J. Miller, H. Jouhara, Development and analysis of a packaged trilateral flash cycle system for low grade heat to power conversion applications, Therm. Sci. Eng. Prog. 4 (2017) 113–121, doi:10.1016/j.tsep.2017.09.009.
[12] D.G. Elliott, E. Weinberg, Acceleration of Liquids in Two-Phase Nozzles, Technical Report 32–987, California Institute of Technology, California, U.S., 1968.
[13] D.G. Elliott, Theory and Tests of Two-Phase Turbines, Technical Report DOE–ER–10614–1, Jet Propulsion Laboratory, California Institute of Technology, California, U.S., 1982.
[14] A. Spinelli, G. Cammi, C.C. Conti, S. Gallarini, M. Zocca, F. Cozzi, P. Gaetani, V. Dossena, A. Guardone, Experimental observation and thermodynamic modeling of non-ideal expanding flows of siloxane MDM vapor for ORC applications, Energy 168 (2019) 285–294, doi:10.1016/j.energy.2018.11.071.
[15] A. Uusitalo, T. Turunen-Saaresti, J. Honkatukia, R. Dhanasegaran, Experimental study of small scale and high expansion ratio ORC for recovering high temperature waste heat, Energy 208 (2020) 118321, doi:10.1016/j.energy.2020.118321.
[16] A. Head, Novel experiments for the investigation of non-ideal compressible fluid dynamics: the ORCHID and first results of optical measurements, Delft University of Technology, 2021 PhD.
[17] F. Alshammari, A. Pesyridis, Experimental study of organic rankine cycle system and expander performance for heavy-duty diesel engine, Energy Convers. Manage. 199 (2019) 111998, doi:10.1016/j.enconman.2019.111998.
[18] F. Reinker, R. Wagner, L. Hake, S. aus der Wiesche, High subsonic flow of an organic vapor past a circular cylinder, Exp. Fluids 62 (3) (2021) 1–16, doi:10.1007/s00348-021-03158-y.
[19] M.T. White, Cycle and turbine optimisation for an ORC operating with two-phase expansion, Appl. Therm. Eng. 192 (2021) 116852, doi:10.1016/j.applthermaleng.2021.116852.
[20] M.T. White, T. Turunen-saaresti, Simulation of a supersonic stator vane under two-phase inlet conditions, in: 6th International Seminar on ORC Power Systems, 11–13 October, Munich, Germany, 2021, pp. 1–8,Paper ID: 13, doi:10.14459/2021mp1632898.
[21] E.O. Sampedro, L. Védie, Wet to dry cycles for high temperature waste heat valorisation using a diphenyl-biphenyl oxide mixture, in: 6th International Seminar on ORC Power Systems, 11–13 October, Munich Germany, 2021, pp. 1–10,Paper ID: 57, doi:10.14459/2021mp1633030.
[22] Y. Liao, D. Lucas, 3D CFD simulation of flashing flows in a converging-diverging nozzle, Nucl. Eng. Des. 292 (2015) 149–163, doi:10.1016/j.nucengdes.2015.06.015.
[23] S. Rane, L. He, Numerical analysis of a novel two-phase turbine using thermal non-equilibrium, homogeneous nucleation phase change, Therm. Sci. Eng. Prog. 22 (December 2020) (2021), doi:10.1016/j.tsep.2020.100827.
[24] S. Dykas, W. Wróblewski, Two-fluid model for prediction of wet steam transonic flow, Int. J. Heat Mass Transf. 60 (1) (2013) 88–94, doi:10.1016/j.ijheatmasstransfer.2012.12.024.
[25] C. Lettieri, D. Yang, Z. Spakovszky, An investigation of condensation effects in supercritical carbon dioxide compressors, J. Eng. Gas Turbine Power 137 (8) (2015) 82602, doi:10.1115/1.4029577.
[26] A. Romei, G. Persico, Computational fluid-dynamic modelling of two-phase compressible flows of carbon dioxide in supercritical conditions, Appl. Therm. Eng. 190 (2021) 116816, doi:10.1016/j.applthermaleng.2021.116816.
[27] F. Giacomelli, F. Mazzelli, A. Milazzo, A novel CFD approach for the computation of R744 flashing nozzles in compressible and metastable conditions, Energy 162 (2018) 1092–1105, doi:10.1016/j.energy.2018.08.050.
[28] G. Besagni, Ejectors on the cutting edge: the past, the present and the perspective, Energy 170 (2019) 998–1003, doi:10.1016/j.energy.2018.12.214.
[29] H. Chen, D.Y. Goswami, E.K. Stefanakos, A review of thermodynamic cycles and working fluids for the conversion of low-grade heat, Renew. Sustain. Energy Rev. 14 (9) (2010) 3059–3067.
[30] C. Invernizzi, P. Iora, P. Silva, Bottoming micro-Rankine cycles for micro-gas turbines, Appl. Therm. Eng. 27 (1) (2007) 100–110, doi:10.1016/j.applthermaleng.2006.05.003.

[31] J. Rijpkema, K. Munch, S.B. Andersson, Thermodynamic potential of twelve working fluids in Rankine and flash cycles for waste heat recovery in heavy duty diesel engines, Energy 160 (2018) 996–1007, doi:10.1016/j.energy.2018.07.003.
[32] H. Städtke, Gasdynamic Aspects of Two-Phase Flow, Wiley-VCH Verlag GmbH & Co. KGaA, Weinheim, 2006.
[33] ANSYS, CFX-solver theory guide, Version 18, Pennsylvania, U.S.(2020).
[34] W. Ranz, W. Marshall, Evaporation from drops - Parts I and II, Chem. Eng. Prog. 48 (1952). 141–146; 173–180.
[35] L. Schiller, A. Naumann, A drag coefficient correlation, Z. Ver. Dtsch. Ing. 77 (1935) 318–320.
[36] D.R. Guildenbecher, C. López-Rivera, P.E. Sojka, Secondary atomization, Exp. Fluids 46 (2009) 371–402, doi:10.1007/s00348-008-0593-2.
[37] J.P. Janet, Y. Liao, D. Lucas, Heterogeneous nucleation in CFD simulation of flashing flows in converging-diverging nozzles, Int. J. Multiphase Flow 74 (2015) 106–117, doi:10.1016/j.ijmultiphaseflow.2015.04.005.
[38] M.E. Mondéjar, M.O. Mclinden, E.W. Lemmon, Thermodynamic properties of trans-1-chloro-3,3,3-trifluoropropene (R1233zd(E)): vapor pressure, (p, ρ, T) behaviour, and speed of sound measurements, and equation of state, J. Chem. Eng. Data 60 (8) (2015) 2477–2489, doi:10.1021/acs.jced.5b00348.
[39] M. Thol, F.H. Dubberke, G. Rutkai, T. Windmann, A. Köster, R. Span, J. Vrabec, Fundamental equation of state correlation for hexamethyldisiloxane based on experimental and molecular simulation data, Fluid Phase Equilib. 418 (2016) 133–151, doi:10.1016/j.fluid.2015.09.047.
[40] M. White, A. Sayma, A generalised assessment of working fluids and radial turbines for non-recuperated subcritical organic rankine cycles, Energies 11 (4) (2018) 800, doi:10.3390/en11040800.